



HAL
open science

Modulated Multipolar Structures in Magnetic Arrays

Elena Vedmedenko, Roland Wiesendanger

► **To cite this version:**

Elena Vedmedenko, Roland Wiesendanger. Modulated Multipolar Structures in Magnetic Arrays. *Philosophical Magazine*, 2008, 88 (18-20), pp.2683-2697. 10.1080/14786430802331199. hal-00513937

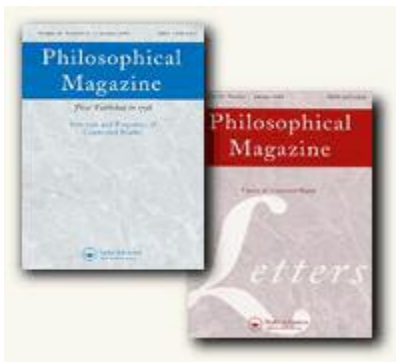
HAL Id: hal-00513937

<https://hal.science/hal-00513937>

Submitted on 1 Sep 2010

HAL is a multi-disciplinary open access archive for the deposit and dissemination of scientific research documents, whether they are published or not. The documents may come from teaching and research institutions in France or abroad, or from public or private research centers.

L'archive ouverte pluridisciplinaire **HAL**, est destinée au dépôt et à la diffusion de documents scientifiques de niveau recherche, publiés ou non, émanant des établissements d'enseignement et de recherche français ou étrangers, des laboratoires publics ou privés.



Modulated Multipolar Structures in Magnetic Arrays

Journal:	<i>Philosophical Magazine & Philosophical Magazine Letters</i>
Manuscript ID:	TPHM-08-May-0158.R1
Journal Selection:	Philosophical Magazine
Date Submitted by the Author:	03-Jul-2008
Complete List of Authors:	Vedmedenko, Elena; University of Hamburg, Institute for Applied Physics Wiesendanger, Roland; University of Hamburg, Institute for Applied Physics
Keywords:	magnetic nanoparticles, Monte-Carlo, multiscale modelling
Keywords (user supplied):	magnetic arrays, lattice models, potential theory
<p>Note: The following files were submitted by the author for peer review, but cannot be converted to PDF. You must view these files (e.g. movies) online.</p> <p>PhM_VW_revised.tex EYV_biblio_2008.bib</p>	



Modulated Multipolar Structures in Magnetic Arrays

E. Y. VEDMEDENKO* & R. WIESENDANGER

* Institut for Applied Physics, University of Hamburg, Jungiusstr. 11, 20355 Hamburg, Germany

(May, 2008)

Electric and magnetic multipole moments are important quantities in studies of intermolecular forces, electrostatic and magnetostatic potentials. The experimental determination of multipole moments in multipole-multipole coupling is difficult and therefore the theoretical prediction of these quantities is important. The aim of the present review is to give a general theoretical description of multipolar ordering on two-dimensional periodic and aperiodic lattices. After an introduction to the role of multipolar interactions in magnetic nanoarrays in the first part of this manuscript the static multipole expansion in cartesian and spherical coordinates are outlined. Next, the established numerical approach for the calculation of multipolar ground states; i.e., Monte Carlo simulations are summarized. Special emphasis is put on the review of ground states in multipolar systems consisting of moments of odd parity relevant for the magnetized or polarized particle ensembles. We demonstrate that higher-order interactions considerably change the dipolar ground states of in-plane magnetized arrays. While in periodic triangular, square and kagome arrays the higher order interactions induce three or four-fold in-plane anisotropy, on a Penrose tiling with ten-fold symmetry the multipolar terms do not seriously affect the dipolar order.

1 Introduction

The appearance of new experimental techniques like spin resolved scanning tunnelling microscopy (SP-STM), magnetic force microscopy (MFM), atomic force microscopy (AFM) and magnetic exchange force microscopy (MExFM) enable the fabrication and manipulation of nanosystems and rapid rise of the scientific research on ever-smaller magnets. Exploring the nanoworld has created an urgent need for a quantitative and qualitative understanding of matter at the atomic scale. One of the interesting aspects vividly discussed nowadays is the interparticle interaction in magnetic nanoarrays. Magnetic properties of artificially structured and self-organized magnetic media belong to the central questions of nanomagnetism as they give access to new phenomena that can be used in technology for a number of applications as storage, high speed non-volatile magnetic memory (MRAM), and logic functions for computations [1–4]. Different applications require different properties of an array. While in storage applications every particle should be addressed individually; *i.e.* the nanoelements should not interact, for logic schemes strong interactions are necessary. In both cases the control of interactions between nanoparticles is crucial.

To identify effects of long-range interaction on magnetic behavior extensive experimental [3–9] and theoretical [10–12] studies of magnetic nanoarrays have been performed. The derivation of the theory of these interactions requires knowledge of the magnetic charge distribution of a particle. Recently it has been demonstrated that one of the simplest and effective ways to do this is to describe a distribution of charges as a series of multipole moments [13, 14].

The magnetic moment (magnetic charge) of an island is determined by the magnetization distribution in the interior of a particle, its shape, the single- or polycrystalline character, and so on. For example, the magnetic moment of a sphere which is homogeneously magnetized along one of its principal axes is identical to that of an equivalent dipole positioned at its center. At the same time the magnetic moment of a homogeneously magnetized rhombic prism possess higher order multipolar contributions [15]. The higher order multipole terms change the magnetostatic interparticle coupling and, hence, the magnetization reversal in densely packed ensembles of particles [10, 13, 16–18]. When the interdot distance is comparable to the dot size magnetostatic interaction between the dots may introduce cooperative ordering in dot arrays

*Corresponding author. Email: vedmeden@physnet.uni-hamburg.de

and change the nucleation fields due to the stabilization of magnetization near the edges of neighboring particles.

The examples given above underline the importance of knowledge of multipolar phase transitions and ground states for applications as well as for fundamental understanding of physics and chemistry of solid state systems. In this article the collective ordering of magnetostatically coupled ensembles on lattices of different symmetry will be reviewed.

Generally, the magnetic/electric charge distributions of uniformly polarized magnetic and ferroelectric nanoparticles possess a mix of multipolar contributions of the odd rank including dipolar Q_{1m} , octopolar Q_{3m} , dotriacontapolar Q_{5m} and possibly even higher-order terms. However, for certain geometries some of the multipole moments may become extinct. For example, a tetragonal prism with equal height, width, and length—which is therefore a cube—possesses strong dipolar but a zero octopole moment, while its strongly elongated or very flat counterparts have strong octopolar contributions. The dependence of the strength of multipole moments on the effective aspect ratio and shape of a particle can be found in [19,20]. To the experimental systems possessing multipoles of even order belong molecular adsorbates including H_2 , N_2 , CO on salts (e.g. boron nitride) or metal surfaces, organic PTCDA molecules on Ag, and methane on graphite. As our primary interest lies in the description of collective phenomena in magnetic arrays only odd-rank contributions will be addressed below. We start with the outline of basic theoretical techniques. The second part of this review is devoted to the theoretical study of the ground states of magnetostatically interacting periodic nanoarrays, while in the last part frustrated aperiodic multipole arrangements are considered. All calculations described in this paper concern arrays of two-dimensional symmetry like, e.g., a square lattice of magnetic dots. The magnetic moments, however, possess $O(3)$ symmetry. In the following the term "two-dimensional" will be used just in the sense of lattice geometry but not as a full quantum mechanical treatment.

2 Static Multipole Expansion of Interaction Energy in Cartesian and Spherical Coordinates

The collective behavior of magnetic nanoarrays is governed by two main contributions to the magnetostatic interactions: the static coupling between magnetization distributions of individual elements as well as dynamic effects coming from the off-diagonal terms in the interaction matrix due to spin-spin correlations, fluctuations and spin-wave excitations [21]. In the following we focus on the theoretical description of the static part of magnetostatic interactions only.

Beyond the approximation of potentials the framework of multipole expansion allows the calculation of the interaction energy of two charge distributions ρ^A and ρ^B . In the following the charge distributions around A and B are considered *non intersecting*; i.e., two spheres surrounding ρ^A and ρ^B do not overlap. The distance between the two charge distributions is $\vec{R}_{AB} = \vec{r}_{c,B} - \vec{r}_{c,A}$, where $\vec{r}_{c,A}$ and $\vec{r}_{c,B}$ are the centers of charge of ρ^A and ρ^B , respectively. The interaction energy of these distributions is given by

$$4\pi\kappa E_{\text{int}} = \int d\vec{r}_A \int d\vec{r}_B \frac{\rho^A(\vec{r}_A)\rho^B(\vec{r}_B)}{\|\vec{R}_{AB} - \vec{r}_A + \vec{r}_B\|} \quad (1)$$

The two integrations are performed with respect to different coordinate systems; the coordinate axes are chosen to be mutually parallel while the origins are defined by the centers of charge.

In cartesian coordinates the denominator can be rearranged and Taylor expanded.

$$\frac{1}{\|\vec{R}_{AB} - \vec{r}_A + \vec{r}_B\|} = \frac{1}{\|\vec{R}_{AB}\|} \frac{1}{\sqrt{1 + 2\vec{n} \cdot \vec{\tau}_{AB} + \|\vec{\tau}_{AB}\|^2}}, \quad (2)$$

where \vec{n} is the unit vector pointing in direction of \vec{R}_{AB} and $\vec{\tau}_{AB} = \|\vec{R}_{AB}\|^{-1}(\vec{r}_B - \vec{r}_A)$. The square root of Eq. 2 is expanded analogously to $f(x) = (\sqrt{1+x})^{-1}$. Within the expansion one has to identify the

1 multipole moments. For the low order moments; i.e., charge q , dipole \vec{p} , and quadrupole \overleftrightarrow{Q} , one finds

$$\begin{aligned}
 2 \quad 4\pi\kappa E_{\text{int}} &= \frac{q^A q^B}{\|\vec{R}_{AB}\|} + \vec{R}_{AB} \cdot \frac{q^A \vec{p}^B + q^B \vec{p}^A}{\|\vec{R}_{AB}\|^3} + \\
 3 \quad &+ \frac{q^A Q^B + q^B Q^A}{\|\vec{R}_{AB}\|^3} + \frac{\|\vec{R}_{AB}\|^2 \vec{p}^A \cdot \vec{p}^B - 3(\vec{R}_{AB} \vec{p}^A)(\vec{R}_{AB} \vec{p}^B)}{\|\vec{R}_{AB}\|^5} + \\
 4 \quad &+ \mathcal{O}[\|\vec{R}_{AB}\|^{-4}], \tag{3}
 \end{aligned}$$

11 where $2Q^{A,B} = (\vec{n})_i^2 (\overleftrightarrow{Q}^{A,B})_{ii}$ is a direction weighted trace.

12 In spherical coordinates the first step of the expansion is

$$\frac{1}{\|\vec{R}_{AB} - \vec{r}_A + \vec{r}_B\|} = \sum_{L,M} R_{LM}^*(\vec{r}_A - \vec{r}_B) I_{LM}(\vec{R}_{AB}), \tag{4}$$

15 where R_{LM} and I_{LM} are regular and irregular normalized spherical harmonics correspondingly. In the next
 16 step one has to apply the so-called addition theorem to separate \vec{r}_A and \vec{r}_B [22]. Eventually the interaction
 17 energy reads

$$\begin{aligned}
 18 \quad 4\pi\kappa E_{\text{int}} &= \int d\vec{r}_A \rho^A(\vec{r}_A) \int d\vec{r}_B \rho^B(\vec{r}_B) \times \\
 19 \quad &\times \sum_{l_A, l_B, m_A, m_B} (-1)^{l_A} \sqrt{\frac{(2l_A + 2l_B + 1)!}{(2l_A)!(2l_B)!}} R_{l_A m_A}(\vec{r}_A) R_{l_B m_B}(\vec{r}_B) \times \\
 20 \quad &\times I_{l_A + l_B - (m_A + m_B)}(\vec{R}_{AB}) \begin{pmatrix} l_A & l_B & l_A + l_B \\ m_A & m_B & -(m_A + m_B) \end{pmatrix} \\
 21 \quad &= \sum_{l_A, l_B, m_A, m_B} (-1)^{l_A} \sqrt{\frac{(2l_A + 2l_B + 1)!}{(2l_A)!(2l_B)!}} Q_{l_A m_A}^A Q_{l_B m_B}^B \times \\
 22 \quad &\times I_{l_A + l_B - (m_A + m_B)}(\vec{R}_{AB}) \begin{pmatrix} l_A & l_B & l_A + l_B \\ m_A & m_B & -(m_A + m_B) \end{pmatrix}. \tag{5}
 \end{aligned}$$

23 Note that—in contrast to cartesian coordinates—it is very easy to identify the multipole moments $Q_{l_A m_A}^A$
 24 and $Q_{l_B m_B}^B$ of non-intersecting charge distributions A and B .

25 3 Methods

26 Both expressions derived above can be used for the evaluation of the multipolar ground states. For such
 27 complicated, many-sided interactions like multipolar ones the configurational space is very large and the
 28 analytical methods for the description of ground states are often inapplicable. For that reason the Monte
 29 Carlo (MC) approach frequently gives a unique possibility to derive the thermodynamic properties and
 30 ground states of multipolar systems. The MC scheme is based on minimization of a system's free energy by
 31 performing statistical sampling experiments on a computer. Statistical sampling or "importance sampling"
 32 is the technique for picking out the important states from the very large number of possibilities [23, 24].
 33 The general strategy is to pick the states μ not randomly, but with probability $p_\mu = Z^{-1} e^{-\beta E_\mu}$, where Z
 34 is the partition function and $\beta = 1/(k_B T)$ with k_B the Boltzmann constant. In a properly equilibrated
 35 Monte-Carlo system all chosen states have to appear with their correct Boltzmann probability.

36 Generally, both Hamiltonians Eq. (5) or Eq. (3) can be introduced into a MC scheme [23] for the
 37 derivation of the stable low temperature configurations of an ensemble of classical multipolar rotors. The
 38

first order element of the cartesian version of the multipolar interaction tensor (the fourth summand of Eq. 3) is widely used for the numerical description of the dipole-dipole interaction playing an important role in magnetic or polar systems [25–28]. In very few cases [29,30] one uses cartesian representation of the quadrupolar interaction ($\mathcal{O}[\|\vec{R}_{AB}\|^{-4}]$) for energy calculations of certain states of molecular ensembles. However, already the quadrupolar term is never used for MC simulations not to mention the higher order contributions. The main reason for this is that the complexity of calculations drastically increases with increasing order of the expansion. In addition to already rather complicated, long range terms of the dipolar contribution $(\vec{R}_{AB} \cdot \vec{p}^A)(\vec{R}_{AB} \cdot \vec{p}^B)$ expressions like $(\vec{R}_{AB} \cdot \vec{p})^2$ and/or $(\vec{p}^A \cdot \vec{p}^B)^2$ emerge. This leads to additional nested summations and the energy minimization becomes a formidable task.

The spherical coordinates allow a much easier treatment of higher order moments and their interaction energies (see Eq. (5)). For example, the fifth order, dotriacontapole moment has components Q_{5m} with $-5 \leq m \leq 5$ in spherical coordinates while it would be a tensor of the form D_{ijklm} with $(i, j, k, l, m) \in \{x, y, z\}$ in cartesian coordinates. Even though the number of independent tensor components is the same the number of nested summations in the spherical representation does not increase for higher order moments. Therefore, the technique of spherical coordinates is much more appropriate for the MC simulations of ensembles consisting of particles with non-intersecting charge distributions [31–33].

The theoretical treatments of multipolar ground states are still very rare and are mostly restricted to classical, rotationally symmetric multipole moments Q_{lm} with $l = 1..4$ and $m = 0$ (generally $m = -l..l$), where l and m correspond to the two degrees of freedom on a sphere. In order to calculate any order of interactions within reasonable effort often spherical coordinates are used [31, 33]. According to the expression (5) the Hamiltonian of the multipolar interaction reads

$$H = \frac{1}{4\pi\mu_0} \sum_{\substack{A \neq B \\ l_A l_B m_A m_B}} T_{l_A l_B m_A m_B}(\vec{R}_{AB}) Q_{l_A m_A}^A Q_{l_B m_B}^B \quad (6)$$

where $Q_{l_A m_A}^A$ and $Q_{l_B m_B}^B$ are the moments of multipoles A and B expressed in spherical harmonics and $T_{l_A l_B m_A m_B}(\vec{R}_{AB})$ is the geometric interaction tensor depending on the interparticle distance vector \vec{R}_{AB} between multipoles on sites A and B

$$T_{l_A l_B m_A m_B}(\vec{R}_{AB}) = (-1)^{l_B} I_{l_A + l_B m_A + m_B}^*(\vec{R}_{AB}) \times \sqrt{\frac{(l_A + l_B - m_A - m_B)! (l_A + l_B + m_A + m_B)!}{(l_A - m_A)! (l_B - m_B)! (l_A + m_A)! (l_B + m_B)!}}, \quad (7)$$

where the dependency on the distance is given by the complex conjugate of the irregular normalized spherical harmonic function $I_{lm}(\vec{r}) = \sqrt{\frac{4\pi}{2l+1}} \frac{Y_{lm}(\theta, \varphi)}{r^{l+1}}$. The Heisenberg exchange can be added as well.

The most difficult problem encountered in Monte-Carlo simulations is related to the limited and strongly biased sampling of the configurational space occurring when the temperature is lower than the critical temperature of the model. Below the critical temperature the system can be trapped in local minima, separated by energy barriers that are rarely overtaken by thermal fluctuations. Most of the widely used computational methods designed to avoid this problem are simulated annealing [34], genetic algorithms [35], and stochastic tunneling [36]. With increasing sample size these methods become inefficient because of very long relaxation times. To overcome this problem algorithms like cluster flip schemes [37–39] or multicanonical ensemble methods [40–42] have been proposed. Novel Monte-Carlo algorithms for large systems use a random walk in energy space instead of the configurational space to obtain a very accurate estimate of the density of states for classical statistical models [43, 44].

The MC simulations of multipolar systems are still very rare. For that reason and because many of multipolar ground states are strongly non-collinear the cluster algorithms have not been implemented yet for this class of problems. Almost all MC simulations on multipolar ensembles have been done in the framework of the single flip Metropolis scheme with a very slow simulated annealing [32, 33]. In older

calculations the rotational space has been restricted to Ising like or in-plane orientations. In the recent simulations [33] the rotational space was sampled uniformly and was not restricted, i.e. a moment can access any new angle. To avoid metastable states several different simulations of the same system have been performed. Simultaneously starting them at different "seeds" for the random number generator, one ensures that the samples take different paths to the equilibrium. Only when all samples reached the same stable energy level it has been deduced that the system has reached equilibrium.

In addition to effective computational algorithms special attention has to be paid to the calculation of the long-range character of the multipolar interactions. Ideally, for the long-range interactions one needs to calculate the interaction energy between each pair of moments on a lattice. For N moments a CPU time proportional to N^2 per one Monte Carlo step is required in the single spin-flip algorithm. This means that large samples can be treated only with periodic boundary conditions in order to reduce the size of a sample to the size of the periodically repeated unit cell. The periodic boundary conditions are now implemented only for dipolar systems [45]. For higher order multipoles the periodic conditions are not so important because of the faster decrease of the interaction energy as a function of interparticle separation. In addition, the periodic boundaries in many cases can introduce artificial periodicity and other unwanted effects. For those reasons the most part of MC studies on multipolar systems have been performed with open boundary conditions but without any cut-off in interaction; i.e., all pair interactions all over the lattice have been considered [13,33].

To overcome the problem of the very consuming CPU time several alternative approaches have been proposed [27,46,47]. The most straightforward one is the discrete update method of Ref. [27]. Most of the CPU time is consumed for calculating the interaction with far moments. However, when the equilibrium is realized, the change of the effective field in updating individual spins will be small, because the strength of the interactions between two moments decays as R_{AB}^{-2l-1} . Therefore, the effective interaction energy E_i of the site i can be separated into the sum of the interactions up to second-nearest-neighbors E_i^{near} and that from the other moments E_i^{far} . E_i^{near} is then updated for every spin-update trial, while E_i^{far} for every m Monte-Carlo sweeps. In this procedure the CPU time can be reduced by a factor m^{-1} . Combination of the discrete update method with the Fast Fourier Transform (FFT) technique [48] permits even more efficient numerical treatments of dipolar fields for open boundaries [47]. For a dipolar case, using FFT techniques the algorithm needs only of the order of $N \log N$ calculations instead of N^2 calculations which one would need for the straightforward calculation of the double sum in the second summand of Eq. 3. For higher order interactions this method has not been applied so far. Apart from the described scheme a very helpful procedure to increase the efficiency of the slow cooling is an exponential increase of the number of MC steps and/or number of temperature steps with decreasing temperature. At higher temperatures almost each trial move is accepted; i.e., the calculation time per number of MC steps is large. At the same time the relaxation to the equilibrium is quick; i.e., rather few MC steps are needed. At lower temperatures only few moves are accepted and the relaxation time is large. Thus, it is reasonable to use a larger number of MC steps per temperature ($N_{\text{MC}}(T)$) at lower temperatures for a constant amount of temperature steps ($N(T)$) or a larger $N(T)$ for a constant N_{MC} . The latter can be, e.g., accomplished by the function

$$\tau(n) = \tau_2 + (\tau_1 - \tau_2) \frac{e^{-\gamma(n-1)} - e^{-\gamma(N-1)}}{1 - e^{-\gamma(N-1)}}, \quad (8)$$

where $\tau_1 = k_B T_1$ and $\tau_2 = k_B T_2$ are the start and end thermal energy respectively, N is the total number of temperatures steps while γ controls the speed of the exponential temperature decrease. Ideally, both procedures have to be superimposed and the convergence of the relaxation process towards an equilibrium at each temperature step has to be ensured.

The data on critical thermodynamic properties of multipolar systems, which can in principle be obtained from the MC simulations, are very limited even for the dipolar interactions. In a recent MC study of a dipolar ensemble on a triangular lattice with vanishing disorder critical exponents $\alpha = 1.73 \pm 0.02$ and $\gamma = 2.64 \pm 0.1$ have been reported in very good agreement with experimental data on Heusler alloys [49]. Those exponents are very large as compared to values for isotropic 3D ferromagnets [50]. These first calculations show that the multipolar systems possess a very interesting critical behavior and theoretical

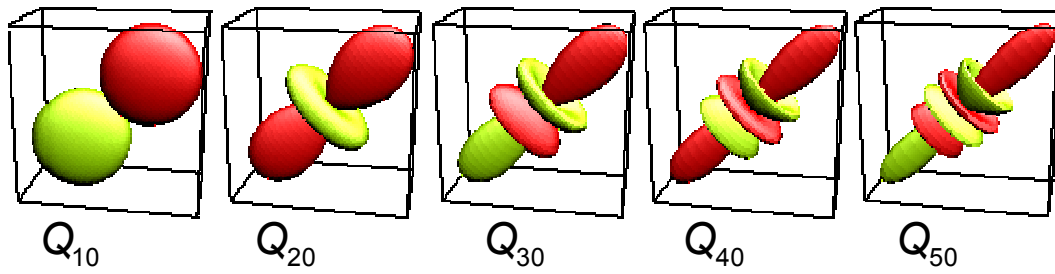


Figure 1. Rotationally symmetric dipole (Q_{10}), quadrupole (Q_{20}), octopole (Q_{30}), hexadecapole (Q_{40}) and dotriacontapole (Q_{50}) in the real spherical harmonic representation.

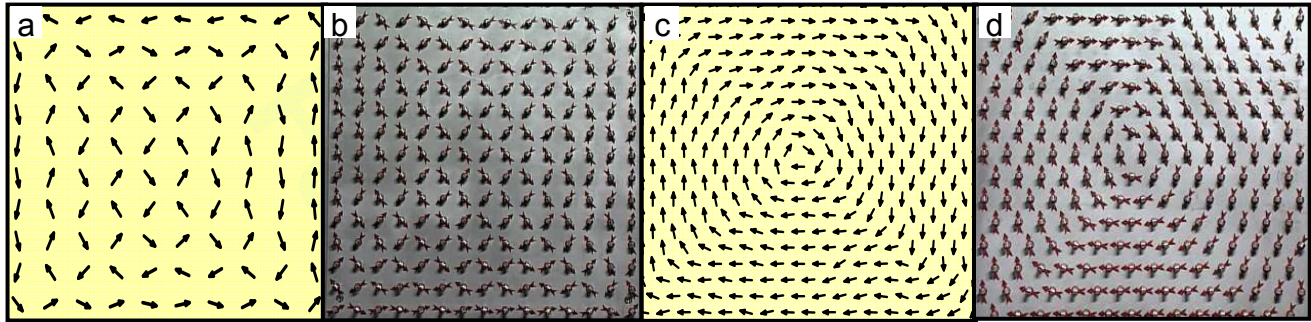


Figure 2. Pure dipolar coupling: top view of (a) a central portion of low-temperature Monte-Carlo configuration on a square lattice ($k_B T = 0.05 E_{dd}$ with E_{dd} dipole-dipole interaction energy); (b) an experimental dipolar model on a square lattice made at the Max-Planck Institute of Microstructure Physics, Halle, Germany; (c) a central portion of low-temperature Monte-Carlo configuration on a triangular lattice ($k_B T = 0.05 E_{dd}$); (d) an experimental dipolar model on a triangular lattice.

predictions on such systems are highly required.

There is no unified representation of multipole moments in the literature. While dipoles are usually represented by arrows it becomes more and more difficult to find similar representation for higher order moments. Therefore the sticks, double arrows etc. are used. We propose to represent all kind of multipoles by real spherical harmonics corresponding to equipotential surfaces of moments. The color of equipotential surfaces reflects the sign of the potential. The first five rotationally symmetric multipole moments in this representation are shown in Fig. 1. An important advantage of the spherical harmonics representation is a very direct visualization of the charge distribution in a system under investigation as will be demonstrated below.

4 Thermodynamic Ground States of Classical, Odd-Parity Multipolar Rotors

This section is devoted to the Monte Carlo results on equilibrium states of magnetic arrays of different geometry. All configurations given in Fig. 2,3,4,5, 6 result from a careful finite size scaling analysis and are thermodynamic ground states. Some of these structures; for example, dipolar configurations on a triangular and a kagome lattice Figs. 2, 4 are very ordered. Another like octopoles on a kagome 4 (b) and a Penrose tiling Fig. 5 possess a significant degree of disorder. Nevertheless, all structures have a minimal possible energy for a given temperature; i.e., they are in thermal equilibrium. Degree of disorder as will be described below is mainly determined by the phase space of each concrete system. In case of ordered structures the thermodynamic ground configuration is unique, while disordered configurations belong to the manifold of energetically degenerated states.

4.1 A Square and a Triangular Lattice

Several studies of dipolar ground state on a square lattice demonstrated that the ground configuration of an infinite square lattice is highly degenerate and defines a continuous manifold of spin configurations at $T = 0$, although the dipolar coupling itself is not rotationally invariant. A typical configuration obtained by Monte-

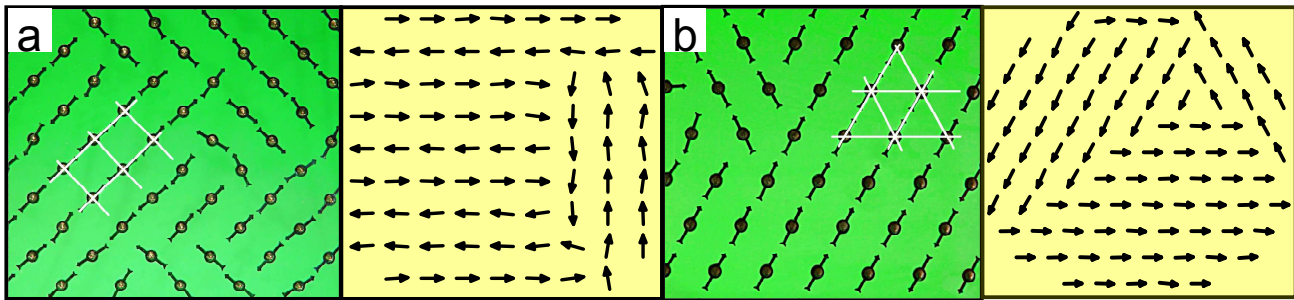


Figure 3. Dipolar and octopolar coupling ($Q_{30} > /Q_{10} = 0.5$):(a) top view of an experimental model and a low-temperature Monte-Carlo configuration on a square lattice($k_{\text{B}}T = 0.05E_{\text{dd}}$ with E_{dd} dipole-dipole interaction energy); (b) the same on a triangular lattice.

Carlo simulations for a finite square lattice at finite temperature is given in Fig. 2(a). Lines of dipoles are observed at the edges which are formed due to the pole avoidance principle. The microvortex configuration is formed in the center. Hence, the finite size and temperature remove the continuous degeneracy of the dipolar ground state on a square lattice.

The ground state of an infinite dipolar array on a triangular lattice is a ferromagnetic-like monodomain structure as follows from Monte-Carlo simulations and mean-field approach. For open boundary conditions a planar vortex structure appears, which is formed to avoid free magnetic poles at the boundaries of the sample (see Fig. 2(c)). In Fig. 2 (b), (d) an experimental model of the square and triangular dipolar arrays is shown. The Monte-Carlo simulations and the experiment reveal identical structures. Thus, due to the geometric frustration of the lattice, which commonly leads to a disorder or a non-collinearity [18], a perfectly ordered vortex on a triangular lattice and an ordered microvortex structure on a square lattice are formed.

While the dipolar ground states on many periodic lattices are known for several decades ground states of two-dimensional arrays of multipoles or their combinations have been considered only recently [33]. The octopolar moments ($Q_{30} \gg Q_{10}$) are unidirectional, i.e. the components of an octopole moment behave themselves like the components of a vector. Therefore, they can be still represented by arrows. It has been found [33] that on a square lattice octopoles form lines being aligned antiparallel while on a triangular lattice the moments are ferromagnetically ordered (see Fig. 3).

As shown in [20], the in-plane magnetized nanodiscs with height-to-diameter ratio $h/a = 0.5$, that are often used in modern experimental studies on nanoarrays, possess dipolar and octopolar moments with $Q_{30}/Q_{10} \approx 0.5$. Hence, for a real nanomagnetic array neither pure dipolar, nor pure octopolar configurations are relevant. Instead, ground states of an ensemble of combined multipoles should be calculated. Our recent results [33] demonstrate that the ground state of a system of particles possessing both multipolar contributions $Q_{10} + Q_{30}$ is similar to a pure octopolar pattern. The main difference is the appearance of rotational domains and alternating regions of parallel and antiparallel chains as can be seen in Fig. 3.

The lines are oriented in principal crystallographic directions. Hence, the octopolar interaction on a triangular and a square lattice introduces an easy-plane and a tri- and a biaxial in-plane anisotropy, respectively. In contrast to finite dipolar systems avoiding uncompensated poles by vortex or domain formation, a finite octopolar system is not sensitive to the formation of free poles in most geometries of a sample. To understand the reason for such a behavior one has to bear in mind that in general dipoles only interact with the field, i.e. the first derivative of the potential $H_i = -\frac{\partial\Phi}{\partial r_i}$. Higher order moments interact with higher derivatives, i.e. quadrupoles with $\frac{\partial^2\Phi}{\partial r_i\partial r_j}$, octopoles with $\frac{\partial^3\Phi}{\partial r_i\partial r_j\partial r_k}$ etc. Hence, octopoles do not interact with a demagnetizing field but with the field curvature. Therefore, the gain in the internal energy due to the compensation of free magnetic poles at the sample boundary is not so strong as for pure dipolar systems and low-temperature configurations in finite samples are still parallel lines for a triangular and antiparallel lines for a square lattice. Thus, the interaction of dipoles with the demagnetizing field is still too weak in comparison to the anisotropy induced due to the octopole-octopole coupling.

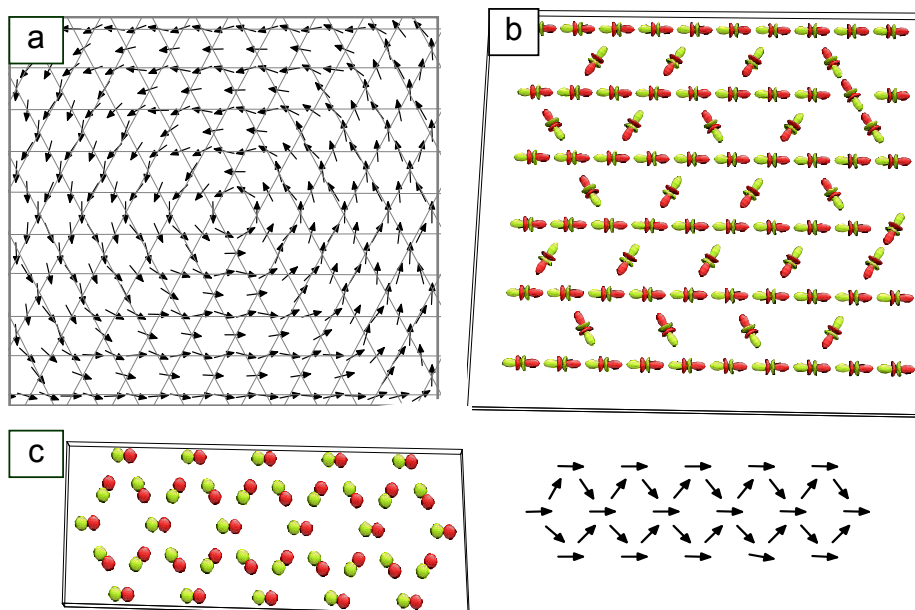


Figure 4. Top-view of a stable dipolar (a) and octopolar (b) configuration on a kagome lattice at $kT = 0.1E_{||}$; (c) the same portion of an infinite dipolar system in arrow and spherical harmonics representation. Different colors mean different surface charges.

4.2 A Kagome Lattice

A kagome symmetry provides a genuine representation of geometric frustration. As well known there is no finite-temperature transition to a phase with a static ordering for an antiferromagnet with only nearest-neighbor exchange interactions on a kagome lattice [51]. It is also well known that the dipolar coupling has an antiferromagnetic nature [52]. On the other hand, in contrast to the direct exchange interactions, any multipolar coupling has a long range character which can significantly change the microscopic ordering of a system. Hence, the question of dipolar and general multipolar ground states on frustrated geometries seems not to be trivial, while it is of great importance due to the increasing number of corresponding two-dimensional experimental systems [53, 54].

In a system of pure dipolar rotors on a kagome lattice a ferromagnetic-like pattern is formed. In an infinite array with periodic boundary conditions a single domain configuration was found while for finite samples a macroscopic planar vortex is obtained as shown in Fig. 4 (a). At first glance the dipolar pattern of Fig. 4 (a) seems to be just a ferromagnetic configuration, slightly disordered by frustration. In reality, however, the situation is more subtle. In Fig. 4 (c) one and the same portion of a pattern is represented with two different visualization techniques. The upper inset gives a usual arrow representation stressing the unidirectionality of the dipoles while at the bottom the equipotential surfaces of the dipolar moments are shown. The color reflects the sign of the potential. The whole pattern can be divided into three sublattices of identical energy but different orientation which can be clearly seen in Fig. 4 (c). The orientation of moments in a sublattice corresponding to more diluted rows coincides with one of the principal crystallographic directions. Two other sublattices make an angle α with the selected orientation. Generally, α depends on the ratio between the dipolar and the exchange coupling. For the pure dipolar case it reaches $\alpha_{max} = (3/4)\pi$ due to the lattice symmetry. Hence, in contrast to an antiferromagnetic system a dipolar ensemble with kagome symmetry shows a stable, unfrustrated behavior.

In the next step we pass to the octopolar rotors on a kagome lattice given in Fig. 4 (b). In spite of the evident similarities of dipolar and octopolar charge distributions a pure octopolar configuration differs ultimately from that of a dipolar one. First, the macroscopic vortex is not formed; second, the ordered sublattices found in a pure dipolar case do not exist; and third, in contrast to the dipolar case the collinear lines are formed along the dense packed rows instead of the looser packed ones. The whole structure is strongly frustrated: a lot of energetically degenerated configurations exist. At low temperatures a system freezes into one of those states. The strong difference between the dipolar and the octopolar ordering stems from the different symmetry of the equipotential surfaces (see Fig. 4 (b)). In contrast to dipoles octopolar

1 moments possess two additional charged "collars" which have to be compensated to decrease the total
2 energy of a system. This requirement forces the parallel alignment of the close packed rows of moments.

3 Similar to previously discussed triangular and square arrays a finite octopolar kagome ensemble is not
4 sensitive to the formation of free poles in most sample geometries. Indeed, while all dipoles at the edge of
5 a finite sample in Fig. 4 (a) are parallel to the sample boundary it is not always the case for octopoles in
6 Fig. 4 (b).
7

8 5 A Penrose Tiling

9
10 While a kagome lattice is frustrated but perfectly periodic, another class of geometrically frustrated, non-
11 periodic systems exists. These are quasicrystals. The quasicrystals can be structurally ranked in-between
12 the periodic lattices and completely disordered media. Starting from the famous pattern of Roger Penrose
13 it has been found many different ways to tile the plane non-periodically with a similar set of regular
14 polygons [55, 56]. Later many of these purely mathematical constructions have found their prototypes in
15 real materials. Nevertheless two most popular quasiperiodic tilings remain the ten-fold Penrose [57] and
16 the eight-fold Ammann-Beenker [58] structures.
17

18 Considering that the magnetic/electric moments are localized on the vertices of a tiling one finds six
19 different types of vertices in a Penrose lattice. For an octagonal tiling eight different local atomic arrange-
20 ments exist. The number of nearest neighbors in quasicrystals varies widely from one vertex to another like
21 in disordered matter. The Penrose tiling, for example, has atoms with coordination number changing from
22 three to seven. Consequently, the energy per magnetic moment in quasicrystals also varies. Several of these
23 vertices are frustrated in the case of antiferromagnetic or dipolar interactions as each rhombic tile consists
24 of two triangles; i.e., magnetic moments are unable to find an orientation satisfying the interactions with
25 all neighbors.
26

27 The frustration in quasicrystals is different from that of periodic systems and that of disordered media.
28 In highly ordered magnets like kagome or pyrochlores the frustration is uniform, i.e., equal for all lattice
29 points. In disordered materials the frustration is random. In quasicrystals the change in coordination
30 number leads to spatial alternation of the local energy and, thus, the degree of frustration. However, the
31 nonuniform magnetic frustration is not random.
32

33 In previous theoretical studies of dipolar ordering (multipole moments of rank one Q_{1m}) on the Penrose
34 tiling, performed in Cartesian coordinates [59], a decagonal pattern with long-range order was proposed as
35 the ground state. Later, after careful and extensive analysis, a clear evidence for short-range order, with
36 very interesting geometric properties, yet no evidence for the emergence of long-range multipolar order
37 has been found [60]. The ground-state configurations of odd-parity multipoles are shown in Fig. 6. At
38 first sight these configurations seem to possess very nice long-range multipolar order, as one clearly sees a
39 superstructure in the form of the familiar decagonal Hexagon-Boat-Star (HBS) tiling shown in Fig. 5 (a).
40 Decagonal rings are clearly visible in both cases, each subdivided into a single boat and a pair of hexagonal
41 tiles. Between the decagons one easily identifies the star-shaped tiles. This aesthetic arrangement of the
42 multipoles found also experimentally (see Fig. 5 (b)) may lead one to the incorrect conclusion that long-
43 range order of the multipoles on the underlying Penrose tiling exists. Yet careful analysis shows that this
44 arrangement stems from the short-range head-to-tail attraction of neighboring multipoles and exhibits no
45 long-range order [60].
46

47 As it turns out, the HBS tiling is simply outlined by pairs and triplets of multipoles that are separated
48 by the short diagonals of the thin (36°) rhombic tiles of the Penrose tiling. This separation, which is the
49 shortest interparticle separation on the Penrose tiling, sets the largest energy scale in the system. As such,
50 these pair and triplet chains are the first to order as the temperature is lowered. Because their positions
51 and orientations are strictly inherited from the Penrose tiling, their ordering on the short scale suffices
52 to outline the HBS tiling that one clearly observes. The existence of short-range order in the orientation
53 of the multipoles is verified quantitatively through a statistical analysis. The absolute orientation of the
54 multipoles, projected onto the plane, is clearly peaked along the 20 directions ($n\pi/10$ for $n = 1 \dots 20$),
55 dictated by the Penrose tiling. The dipolar histogram is more strongly peaked relative to the octopolar one
56 owing to the fact that the octopolar ground state possesses, on average, a larger out-of-plane component.
57
58
59
60

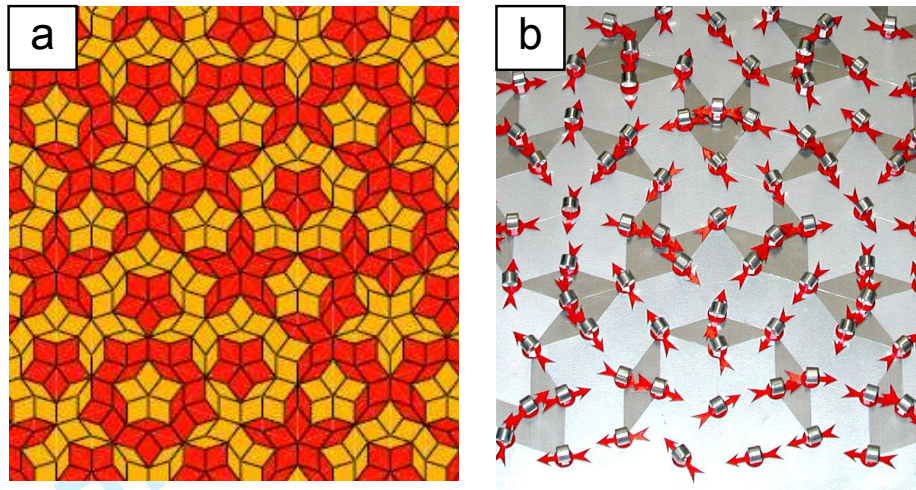


Figure 5. (a) Hexagon-Boat-Star tiling (courtesy of R. Lifshitz); (b) A portion of an experimental dipolar model on the Penrose tiling made at the Max-Planck Institute of Microstructure Physics, Halle, Germany.

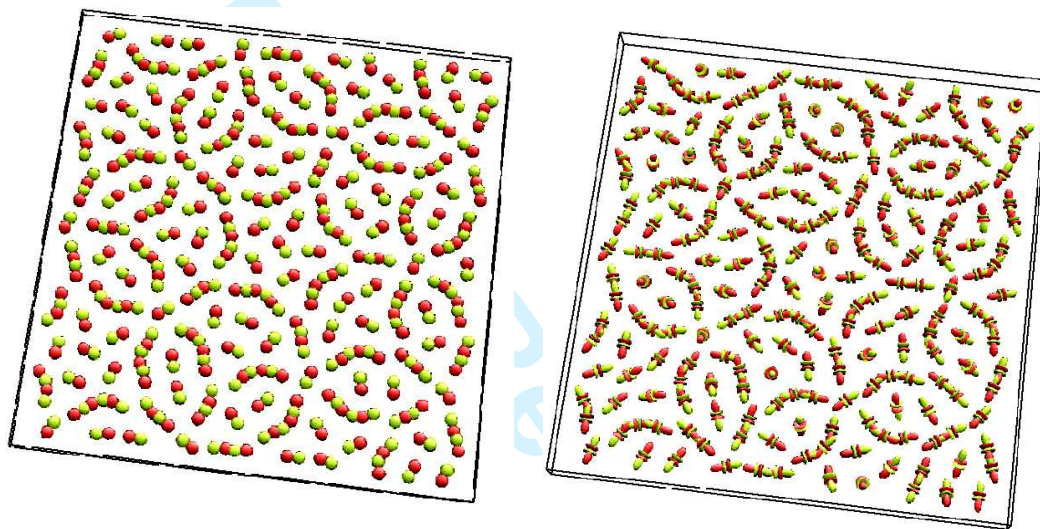


Figure 6. (Color online) Ground-state configurations of odd-parity multipolar rotors. (Left) dipole moments; (Right) octopole moments. These configurations possess short-range order, owing to the strong head-to-tail attraction of neighboring multipoles, which is sufficient to highlight the decagonal Hexagon-Boat-Star Tiling.

A frequency distribution of the angle between nearest neighboring moments is also peaked at the characteristic angles inherited from the relative orientation of thin rhombic tiles on the Penrose tiling, and is significantly less-pronounced for the octopolar moments due to their substantial out-of-plane protrusion. Though the octopolar arrangement contains a larger average out-of-plane component, and a slightly less-perfect short-range order within the plane, the two cases are quite similar. The difference stems from the fact that there is some amount of attraction of the arrow heads to the central oppositely-charged regions of neighboring octopoles (see Fig. 1).

We note that in magnetic systems the strength of the multipolar interactions can be tuned by the shape of the particles, or their size relative to the interparticle separations. The octopolar contribution may become very large for $R_{AB} < s$, with s being the lateral size of a particle. The dipolar contributions are sizable for $R_{AB} < 5s - 10s$. For very small interparticle separations the decagonal structure might become disordered due to the octopolar contributions, while for very large separations disorder may appear because of the weakness of the dipolar coupling. This implies that there exists a critical separation R_{AB}^c for which the short-range ordering of odd-parity multipoles on the Penrose tiling is maximal. For typical particle shapes used in experiments [33] this critical distance is of the order of $1s - 2s$.

The multipoles that lie within the HBS tiles are disordered, as can be verified by simple inspection.

Nevertheless, one could still imagine a situation in which the multipoles that lie on the edges of the HBS tiles are long-range ordered while the internal multipoles are not. Yet upon further inspection one finds that multipoles lying on the edges of the HBS tiles are disordered as well, as their direction changes randomly from one pair or triplet chain to the next. This disorder is a direct consequence of the frustration that arises whenever the ends of three such chains meet together. This can be seen, for example, at the five vertices of the central star tile in both configurations, shown in Fig. 6. The observation of the lack of long-range order is confirmed quantitatively by performing a Fourier analysis of the ground state configurations [60]. By examining the different components of the multipolar fields, as well as various functions of the components, one can say with certainty that such order is lacking, as the calculated Fourier spectra show no additional Bragg peaks when compared to the Fourier spectrum of the tiling itself. Thus, the only long-range order that is observed is related to the positions of the multipoles, inherited from the Penrose tiling, and not to their relative orientation. To verify this conclusion, the Fourier spectrum of a randomly oriented configuration of multipole moments on the vertices of the Penrose tiling, created using a random number generator, has also been calculated. The outcome strongly resembles that of the ground-state configurations.

6 Summary

Low-temperature stable multipolar ordering on a square, a triangular, a kagome lattice and a Penrose tiling has been reviewed. Emphasis has been put on the multipolar contributions of odd parity relevant for ensembles of polarized or magnetized particles. It is demonstrated that the dipolar interactions partially relieve strong frustration characteristic for antiferromagnetic systems on a triangular and a kagome lattice, while dipolar ensembles with a Penrose symmetry possess a manifold of energetically equivalent, frustrated configurations. The pure dipolar coupling leads to a long-range order on periodic lattices and to a short range one on a Penrose tiling. In octopolar tenfold systems the decagonal short range ordering remains but is less pronounced because of frustration arising from the complicated form of the charge distributions. All above mentioned multipolar configurations are at most planar. The octopolar contribution introduces a strong additional three- and four-fold anisotropy on triangular and square lattices, respectively. Tuning the multipole moments by changing the geometry of nanoparticles offers a new route to the control of the coupling behaviour and therefore the hysteretic properties of magnetic nanoparticle arrays.

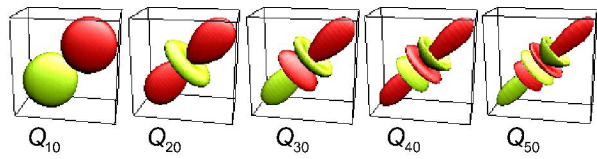
* Financial support from the Deutsche Forschungsgemeinschaft in the framework of the part project A11 of the SFB 668 is gratefully acknowledged.

References

- [1] H. Kronmüller and S. Parkin, editors. *Handbook of Magnetism and Advanced Magnetic Materials*, volume 1-5. Wiley, Weinheim, 2007.
- [2] J. A. C. Bland and B. Heinrich. *Ultrathin Magnetic Structures I*. Springer Verlag, Berlin, 1994.
- [3] T. Aign, P. Meyer, S. Lemerle, J. P. Jamet, J. Ferré, V. Mathet, C. Chappert, J. Gierak, C. Vieu, F. Rousseaux, H. Launois, and H. Bernas. Magnetization Reversal in Arrays of Perpendicularly Magnetized Ultrathin Dots Coupled by Dipolar Interaction. *Phys. Rev. Lett.*, 81:5656, 1998.
- [4] R. P. Cowburn and M. E. Welland. Room temperature magnetic quantum cellular automata. *Science*, 287:1466, 2000.
- [5] R. P. Cowburn, A. O. Adeyeye, and M. E. Welland. Controlling magnetic ordering in coupled nanomagnet arrays. *New J. of Phys.*, 1:16.1, 1999.
- [6] C. A. Ross, M. Hwang, M. Shima, J. Y. Cheng, M. Farhoud, T. A. Savas, Henry I. Smith, W. Schwarzacher, F. M. Ross, M. Redjda, and F. B. Humphrey. Micromagnetic behavior of electrodeposited cylinder arrays. *Phys. Rev. B*, 65:144417, 2002.
- [7] K. Nielsch, R. B. Wehrspohn, R. Barthel, J. Kirschner, S. F. Fischer, H. Kronmüller, T. Schweinböck, D. Weiss, and U. Gösele. High density hexagonal nickel nanowire array. *J. Magn. Mater.*, 249:234, 2002.
- [8] M. R. Scheinfein, K. E. Schmidt, K. R. Heim, and G. G. Hembree. Magnetic order in two-dimensional arrays of nanometer-sized superparamagnets. *Phys. Rev. Lett.*, 76:1541, 1996.
- [9] A. Remhof, A. Schumann, A. Westphalen, H. Zabel, T. Last, U. Kunze, E. Y. Vedmedenko, and N. Mikuszeit. Magnetostatic interactions on a square lattice. *Phys. Rev. B*, 77:134409, 2008. submitted.
- [10] P. Politi and M. G. Pini. Dipolar interaction between two-dimensional magnetic particles. *Phys. Rev. B*, 66:214414, 2002.
- [11] A. J. Bennett and J. M. Xu. Simulating collective magnetic dynamics in nanodisk arrays. *Appl. Phys. Lett.*, 82:2503, 2003.
- [12] P. J. Jensen. Rapid evaluation of oscillating lattice sums. *Ann. Phys. (Leipzig)*, 6:317, 1997.
- [13] E. Y. Vedmedenko. Influence of the lattice discreteness on magnetic ordering in nanostructures and nanoarrays. *Phys. Stat. Sol. (b)*, 244(4):1133–1165, 2007. and the references inside.
- [14] E. Y. Vedmedenko and N. Mikuszeit. Multipolar ordering in electro- and magnetostatically coupled nanosystems. *Chem. Phys. Chem.*
- [15] E. Olive and P. Molho. Thermodynamic study of a lattice of compass needles in dipolar interaction. *Phys. Rev. B*, 58:9238, 1998.

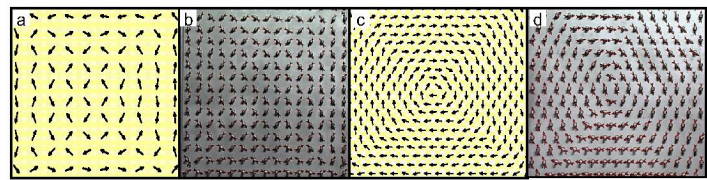
- [16] P. J. Jensen and G. M. Pastor. Low-energy properties of two-dimensional magnetic nanostructures: interparticle interactions and disorder effects. *New J. Phys.*, 5:68, 2003.
- [17] K. Yu. Guslienko. Magnetic anisotropies in two-dimensional arrays induced by magnetostatic interdot coupling. *Phys. Lett. A*, 278:293, 2001.
- [18] E. Y. Vedmedenko. *Competing Interactions and Pattern Formation in Nanoworld*. Wiley, Weinheim, 2007.
- [19] N. Mikuszeit, E. Y. Vedmedenko, and H. P. Oepen. Multipole interaction of polarized single-domain particles. *J. Phys.: Condens. Matter*, 16:9037, 2004.
- [20] N. Mikuszeit, E. Y. Vedmedenko, H. P. Oepen, and R. Wiesendanger. Multipole moments of in-plane polarized disks. *J. Appl. Phys.*, 97:10J502, 2005.
- [21] L. Bergquist and O. Ericksson. Theory of weakly coupled two-dimensional magnets. *J. Phys: Cond. Matter*, 18:4853, 2006.
- [22] A. J. Stone. *The Theory of Intermolecular Forces*. Clarendon Press, Oxford, 1996.
- [23] K. Binder, editor. *The Monte-Carlo method in condensed matter physics*, volume 71 of *Topics in Applied Physics*. Springer, Berlin, 1991.
- [24] M. E. J. Newman and G. T. Barkema. *Monte Carlo Methods in Statistical Physics*. Clarendon Press, Oxford, 1999.
- [25] E. Y. Vedmedenko, A. Ghazali, and J.-C. S. Lévy. Magnetic structures of ising and vector spins monolayers by monte-carlo simulations. *Surf. Sci.*, 402-404:391, 1998.
- [26] D. Hinzke and U. Nowak. Magnetic relaxation in a classical spin chain. *Phys. Rev. B*, 61:6734, 2000.
- [27] J. Sasaki and F. Matsubara. Circular phase of a two-dimensional ferromagnet with dipolar interactions. *J. Phys. Soc. Jpn.*, 66:2138, 1997.
- [28] A. Hucht, A. Moschel, and K. D. Usadel. Monte-carlo study of the reorientation transition in heisenberg models with dipole interactions. *J. Magn. Magn. Mater.*, 148:32, 1995.
- [29] I. E. Dzyaloshinskii, E. I. Kats, and J. Lajzerowocz. Quadrupolar forces and aggregation of nematic droplets. *JETP Letters*, 68:785, 1998.
- [30] V. E. Klymenko, V. M. Rozenbaum, V. V. Kukhtin, and O. V. Schramko. Stabilization of the long-range order within a square dipole lattice by the quadrupole interaction. *Sol. State Comm.*, 88:373, 1993.
- [31] P. Popelier and D. Kosov. Atom-atom partitioning of intramolecular and intermolecular Coulomb energy. *J. Chem. Phys.*, 114:6539, 2001.
- [32] S. F. O'Shea. A monte carlo study of the classical octopolar solid. *J. Chem. Phys.*, 68(12):5435, 1978.
- [33] E. Y. Vedmedenko, N. Mikuszeit, H. P. Oepen, and R. Wiesendanger. Multipolar ordering and magnetization reversal in two-dimensional nanomagnet arrays. *Phys. Rev. Lett.*, 95:207202, 2005.
- [34] S. Kirkpatrick, C. Gelatt Jr., and M. Vecchi. Optimization by simulated annealing. *Science*, 220:671, 1983.
- [35] J. Holland. *Adaptation in Natural and Artificial Systems*. The University of Michigan Press, Ann Arbor, 1975.
- [36] W. Wenzel and K. Hamacker. Stochastic tunneling approach for global minimization of complex potential energy landscapes. *Phys. Rev. Lett.*, 82:3003, 1999.
- [37] R. H. Swendsen and J.-S. Wang. Nonuniversal critical dynamics in monte carlo simulations. *Phys. Rev. Lett.*, 58:86, 1987.
- [38] U. Wolff. Collective monte carlo updating for spin systems. *Phys. Rev. Lett.*, 62:361, 1989.
- [39] E. Luijten and H. W. J. Blöte. Monte carlo method for spin models with long-range interactions. *Int. J. Mod. Phys. C*, 6:359, 1995.
- [40] B. A. Berg and T. Neuhaus. Multicanonical ensemble: A new approach to simulate first-order phase transitions. *Phys. Rev. Lett.*, 68:9, 1992.
- [41] B. A. Berg. Multicanonical recursions. *J. Stat. Phys.*, 82:323, 1996.
- [42] J. Lee. New monte carlo algorithm: Entropic sampling. *Phys. Rev. Lett.*, 71:211, 1993.
- [43] F. Wang and D. P. Landau. Determining the density of states for classical statistical models: A random walk algorithm to produce a flat histogram. *Phys. Rev. E*, 64:056101, 2001.
- [44] S. W. Davis, W. McCausland, H. C. McGahagan, C. T. Tanaka, and M. Widom. Cluster-based monte carlo simulation of ferrofluids. *Phys. Rev. E*, 59:2424, 1999.
- [45] D. C. Rapaport. *The art of molecular dynamics simulations*. Cambridge University Press, 1995.
- [46] E. Y. Vedmedenko, A. Ghazali, and J.-C. S. Lévy. Magnetic vortices in ultrathin films. *Phys. Rev. B*, 59:3329, 1999.
- [47] D. Hinzke and U. Nowak. Magnetization switching in nanowires: Monte carlo study with fast fourier transformation for dipolar fields. *J. Magn. Magn. Mater.*, 221:365, 2000.
- [48] D. V. Berkov, K. R. Ramstock, and A. Hubert. Solving micromagnetic problems - towards an optimal numerical-method. *Phys. Stat. Sol. (a)*, 137:207, 1993.
- [49] Jürgen Kötzler, Detlef Görlitz, Malte Kurfiß, Lars von Sawilski, and Elena Y. Vedmedenko. Vortex fluctuations and freezing of dipolar-coupled granular moments in thin ferromagnetic films. *Phys. Rev. B*, 73:224425, 2006.
- [50] H. E. Stanley. *Introduction to Phase Transitions and Critical Phenomena*. Oxford University Press, London, 1971.
- [51] A. P. Ramirez. *Handbook of Magnetic Materials*, volume 13, page 243. Elsevier Science, North-Holland, 2001.
- [52] K. De'Bell, A. B. MacIsaac, I. N. Booth, and J. P. Whitehead. Dipolar-induced planar anisotropy in ultrathin magnetic films. *Phys. Rev. B*, 55:15108, 1997.
- [53] J. Atwood. *Nature materials*, 1:91, 2002.
- [54] V. Elser. *Phys. Rev. Lett.*, 62:2405, 1989.
- [55] C. L. Henley. *Quasicrystals: The State of the Art*, page 429. World Scientific, Singapore, 1991.
- [56] D. P. DiVincenzo and P. J. Steinhardt. *Quasicrystals The State of the Art*. World Scientific, Singapore, 1991.
- [57] R. Penrose. *Bull. Inst. Math. Appl.*, 10:266, 1974.
- [58] R. Ammann, B. Grünbaum, and G.C. Shephard. *Discrete Comput. Geom.*, 8:1, 1992.
- [59] E. Y. Vedmedenko, H. P. Oepen, and J. Kirschner. *Phys. Rev. Lett.*, 90:137203, 2003.
- [60] E. Y. Vedmedenko, S. E.-D. Mandel, and R. Lifshitz. In search of multipolar order on the penrose tiling. *Phil. Mag.*, 2008. Accepted for publication.

1
2
3
4
5
6
7
8
9
10
11
12
13
14
15
16
17
18
19
20
21
22
23
24
25
26
27
28
29
30
31
32
33
34
35
36
37
38
39
40
41
42
43
44
45
46
47
48
49
50
51
52
53
54
55
56
57
58
59
60



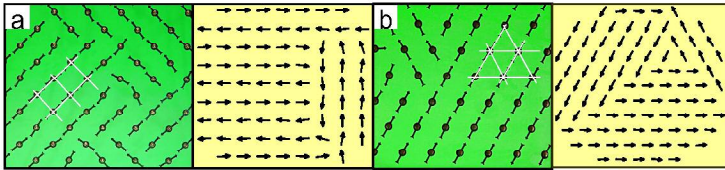
209x297mm (600 x 600 DPI)

1
2
3
4
5
6
7
8
9
10
11
12
13
14
15
16
17
18
19
20
21
22
23
24
25
26
27
28
29
30
31
32
33
34
35
36
37
38
39
40
41
42
43
44
45
46
47
48
49
50
51
52
53
54
55
56
57
58
59
60



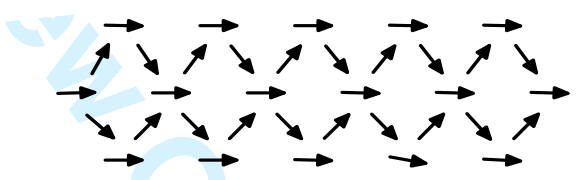
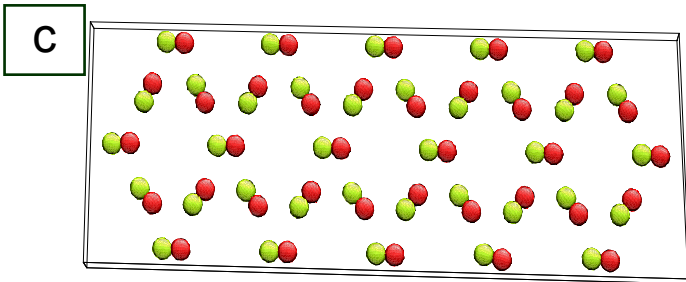
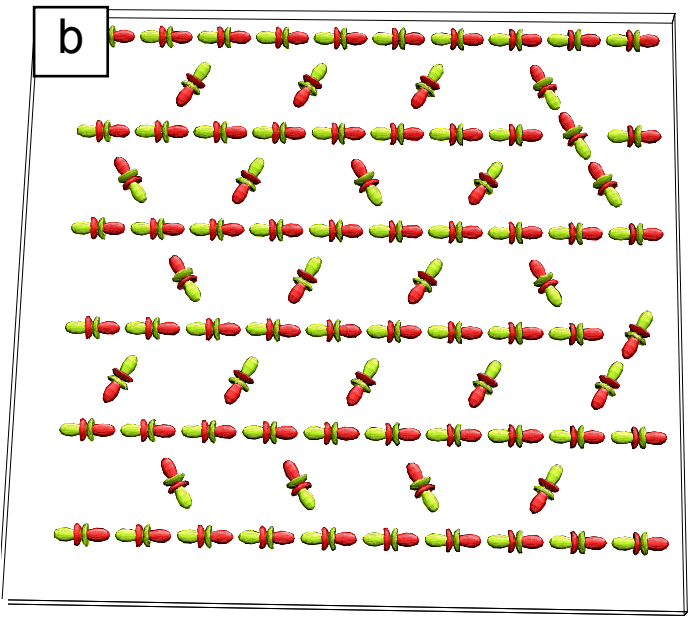
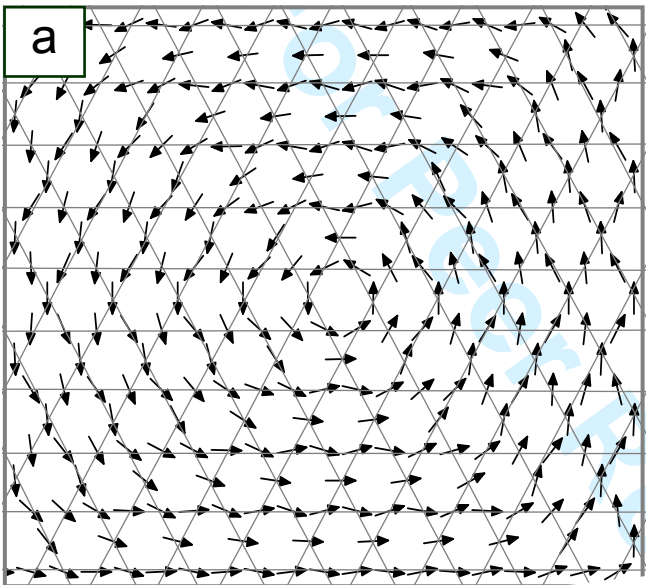
209x297mm (600 x 600 DPI)

1
2
3
4
5
6
7
8
9
10
11
12
13
14
15
16
17
18
19
20
21
22
23
24
25
26
27
28
29
30
31
32
33
34
35
36
37
38
39
40
41
42
43
44
45
46
47
48
49
50
51
52
53
54
55
56
57
58
59
60

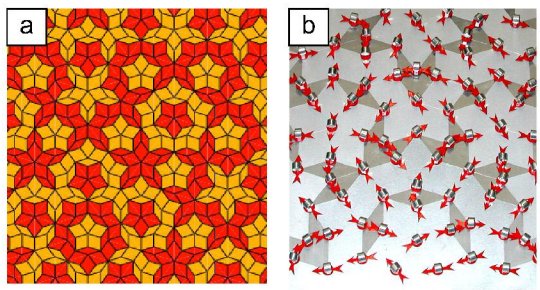


209x297mm (600 x 600 DPI)

1
2
3
4
5
6
7
8
9
10
11
12
13
14
15
16
17
18
19
20
21
22
23
24
25
26
27
28
29
30
31
32
33
34
35
36
37
38
39
40
41
42
43
44
45
46
47
48
49
50
51
52
53
54
55
56
57
58
59
60

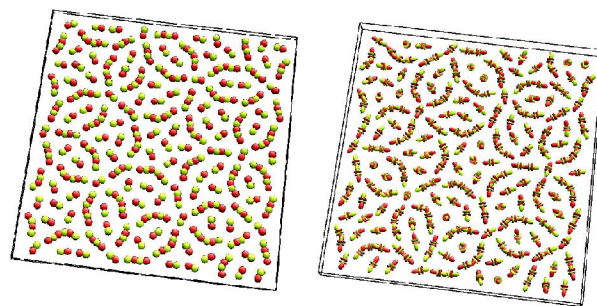


1
2
3
4
5
6
7
8
9
10
11
12
13
14
15
16
17
18
19
20
21
22
23
24
25
26
27
28
29
30
31
32
33
34
35
36
37
38
39
40
41
42
43
44
45
46
47
48
49
50
51
52
53
54
55
56
57
58
59
60



209x297mm (600 x 600 DPI)

1
2
3
4
5
6
7
8
9
10
11
12
13
14
15
16
17
18
19
20
21
22
23
24
25
26
27
28
29
30
31
32
33
34
35
36
37
38
39
40
41
42
43
44
45
46
47
48
49
50
51
52
53
54
55
56
57
58
59
60



209x297mm (600 x 600 DPI)